Identification of a Nonlinear Dielectric Elastomer Actuator Based on the Harmonic Balance Method

Jakub Bernat[1] *Member, IEEE,* Jakub Kolota[1] and Samuel Rosset[2] *Member, IEEE,*

***Abstract*—This paper presents a control-oriented modelling of a circular dielectric elastomer actuator loaded with a mass. Precise dynamic position control of these actuators is a challenge, because of the high level of nonlinearities. Our model takes into account nonlinear mechanical phenomena such as hyperelasticity and viscoelasticity. The behavior of dielectric elastomer actuators is analyzed by a series of experiments on three actuators with different parameters. Furthermore, the model parameters are found using optimization procedures. To improve the performance of the optimization, the steady state solution is found using the Harmonic Balance Method. Compared to a forward integration method, the time gain of the Harmonic Balance Method is significant, and exceeds 2 orders of magnitude when 6 or less harmonics are considered. The application of steady state solver enables taking the frequency response into account for the parameter identification procedure. The results obtained from the model are compared with experiments and show an excellent agreement.**

***Index Terms*—Dielectric Electroactive Polymer, Dielectric Elastomer Actuator, Parameter Identification, Optimization, Harmonic Balance Method**

I. INTRODUCTION

Electroactive Polymers (EAP) are a class of promising smart materials that react to electrical stimuli with a deformation. Dielectric Elastomer Actuators (DEA) are a subclass of the EAP family for which actuation is produced by an elastic deformation resulting from the compressive electrostatic forces caused by charges on the surface of the membrane [1]–[4]. They consist of a thin elastomer membrane (usually silicone), stretched on a frame and sandwiched between two stretchable electrodes, thus forming a deformable rubbery capacitor [3], [5], [6]. The application of an electrical potential between the electrodes, leads to the generation of a Maxwell pressure. This causes a compression of the membrane, and – owing to the incompressibility of elastomers – leads to an increase of the electrode surface. Accurate information about the properties and control methods of DEAs is critical to designers who are considering the construction of mechanisms or devices using these materials. Prototypes of DEA pumps, valves, robots, lens element actuators and micropositioning stages have been documented in recent literature [1], [7]–[10]. DEAs are an interesting solution for positioning applications, thanks to their large output strain, but precise position control is very difficult due to their complex electro-viscomechanical coupling and intrinsic nonlinearities [11]–[14]. Therefore, the accurate operation of DEAs requires an adequate control system.

Many models have been published to describe the dynamic behaviour of DEAs. For example, the Ogden model can be used to model the hyperelastic behaviour of the elastomer, together with a Kelvin-Voigt model to account for the viscous losses in the material [11], [13]. The electrical model of DEAs takes into account the Maxwell Stress Tensor as a coupling force [11]–[13]. The dynamics of the electrical circuit is usually modelled by representing the actuator as a capacitance with a series resistance representing the electrodes. Because of the complexity of the nonlinear processes in play, finite element analysis is often used to study the behaviour of dielectric elastomer actuators [15]–[18]. The main drawback of DEAs is their high driving voltage, which calls for custom-made power supplies [19], [20]. But despite this, DEAs are a very attractive solution for many application fields.

The most important challenge of modeling is posed by the identification of the model parameters [11]–[13]. In experiments with DEAs the most common output is displacement or output force. Hence, the velocity and internal state of the viscoelasticity model are unavailable during identification. Furthermore, the model is nonlinear, because of the mechanical properties of elastomers, and the quadratic relationship between the applied voltage and Maxwell pressure. Consequently, identification procedures commonly used for linear systems are not applicable [21], and optimization approaches are therefore the most reliable identification methods. The application of the identification process to DEAs has been reported in the literature [13], [22], [23]. In general, the identification process is split into two steps. Firstly, the parameters related to the static characteristics are found, for instance with genetic algorithms [22]. Then, the parameters related with the model dynamics are identified, which is a much more complex task. In the works of Zou and Gu, [22] and Gupta et al. [23], expert knowledge about the behavior of the system is required to find the parameters by a trial and error method. In the work of Rizello et al. [13], a nonlinear optimization procedure is applied to identify the parameters.

We have noticed that the dynamics of DEAs consists of oscillations and slow poles due to the relaxation processes of the viscoelasticity. In this work, we take into account the frequency response in the parameter identification procedure. However, in the case of slow poles, using the steady state solution is a time-consuming task, because of the time required to reach steady-state. Hence, an alternative approach is required to tackle this challenge. In this contribution, we introduce the use of the Harmonic Balance Method (HBM) [24], [25] to identify the response of DEAs. The harmonic balance

[1]Jakub Bernat and Jakub Kolota are with Faculty of Control, Robotics and Electrical Engineering, Poznan University of Technology, 60-965 Poznan, Poland Jakub.Bernat@put.poznan.pl

[2]Samuel Rosset is with Auckland Bioengineering Institute, The University of Auckland s.rosset@auckland.ac.nz

*This work was realized with the frame of project SONATA 13 No. 2017/26/D/ST7/00092 from National Science Centre (Poland).

principle is the base of a series of methods to search for the solutions of nonlinear dynamic systems. It is very useful in the analysis of chaotic, mechanical, and electromechanical systems [26]–[28]. One of the two approaches of the HBM relies on solving the analytical equations taking into account that the response and excitation are represented as Fourier Series [25]. The second approach is to find the solution based on nonlinear optimization techniques [29]. Besides rapid screening for the steady state solution, it is also possible to use the HBM to analyze important phenomena like Duffing-oscillators [28]. Here, we apply the HBM to identify the parameters of our model from the measured response of DEAs, using the nonlinear optimization approach. This enables us to drastically speed-up the parameter identification process for a sinusoidal excitation by more than two orders of magnitude (c.f. section IV-E).

This paper presents a model of DEAs biased by a mass. In our work, we consider a special case of a generalized Maxwell model for the viscoelastic response, combined with an hyperelastic model for the steady-state mechanical behaviour of the elastomer. The experimental validation is performed on three different types of DEAs membranes. The first two were fabricated by the authors, and the third one was a commercial sample from Leap Technology. This enables a more comprehensive analysis of the optimization procedure.

The remainder of this paper is organized as follows. Section II describes the DEA working configuration and its nonlinear model. In Section III, the HBM method is presented and applied to the DEA model. Section IV the identification procedure is described and validated with a set of experiments. This section highlights the important features of the HBM method applied to the modelling of DEAs.

II. DIELECTRIC ELASTOMER ACTUATORS

DEAs are electromechanical devices, and therefore exhibit an electromechanical coupling, transforming electrical energy into mechanical energy. Their mechanical behaviour is visco-elastic, with the elastic part governed by an hyperelastic strain energy function [13], [30], [31]. These phenomena play important roles in the design of devices using these membranes, and they must be taken into account to accurately build control-oriented models. We explain the basic actuation principle, and then introduce the specific actuator geometry. The actuators presented in this paper are made of a circular membrane stretched over a circular frame. The membrane is placed horizontally, and a mass is fixed at its center, thus creating a biasing force that causes the membrane to deform out-of-plane in a conical shape. The application of a voltage alters the vertical position of the mass. The DEA membrane geometry is shown in Fig. 1. We consider the voltage applied to the membrane as input and the vertical displacement of the mass as output. The DEA membrane is made of an elastomeric membrane which is equi-biaxially prestretched by a factor λ_p during fabrication. Electrodes are then applied on both side of the membrane. They are considered to be perfectly compliant, and their influence is therefore not taken into account in the model.

A. Model

Control-oriented models of DEAs have previously been published, for example in [11]–[13]. Here, we combine the models developed by the group of Stefan Seelecke [13], [32], [33], as well as our own work [34]. These references proposed a dynamic model composed of a set of nonlinear, time-invariant differential equations describing the dynamic relationship between the input voltage and the output actuator displacement. But whereas [13], [32], [33] used a spring to create the initial out-of-plane bias, we present a modified model which considers an inertial mass as a load. This causes a change in the force equation, whose goal is to accurately describe the behavior of the actuator, both in transient and steady state, and for different mass loads. Using a mass bias is one possible configuration, which we choose to demonstrate the identification process using the HBM. In a similar way, the diaphragm actuator used in the study is one particular geometry, but the method can be generalised to other DEA geometries (stacked actuators, rolled actuators, in-plane actuators, etc.)

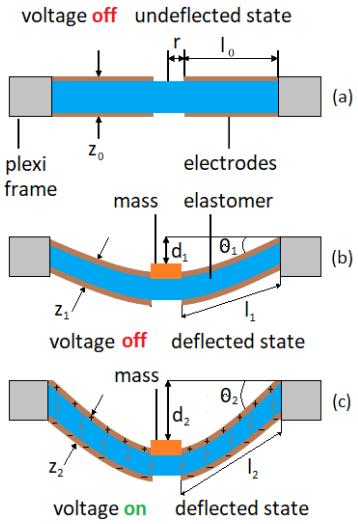

Fig. 1. Dielectric elastomer actuator geometry and working principle. a) Without voltage and mass, b) without voltage and with mass, and c) with applied voltage and mass.

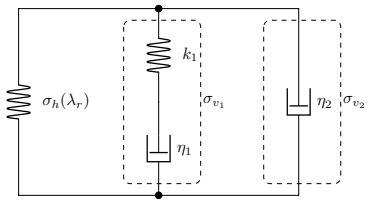

Fig. 2. The components of the mechanical stress (the hyperelastic stress σ_h, the viscoelastic stress σ_{v_1} and the viscous damper stress σ_{v_2}) in the DEA membrane.

Elastomer are considered to deform with a constant volume [1], [7]. Therefore:

$$\lambda_r \lambda_c \lambda_z = 1 \tag{1}$$

where

$$\lambda_r = \frac{l}{l_0} = \frac{\sqrt{l_0^2 + d^2}}{l_0}, \lambda_z = \frac{z}{z_0}, \lambda_c = 1 \tag{2}$$

$$z = z_0 \frac{l_0}{l} = z_0 \frac{l_0}{\sqrt{l_0^2 + d^2}} \tag{3}$$

$$sin(\theta) = \frac{d}{\sqrt{l_0^2 + d^2}} \tag{4}$$

The variables λ_r, λ_c and λ_z are the actuation stretches that are defined relative to the initial prestretch membrane on the frame before any out-of-plane deformation (c.f. Fig. 1). The indexes r, c, and z refer to the radial, circumferential, and vertical direction. That means that the total stretch of the material is given by $\lambda_{r,tot} = \lambda_r \lambda_p$, $\lambda_{c,tot} = \lambda_c \lambda_p$, $\lambda_{z,tot} = \lambda_z / \lambda_p^2$, where λ_p is the equi-biaxial prestretch that is applied to the membrane prior to attaching it to the circular frame (c.f. section IV-A). The parameter z_0 is the initial thickness of membrane (undeflected state), l_0 is the initial length of the electrode (undeflected state), z is the thickness of membrane (deflected state), l is the length of the electrode (deflected state), d is the vertical displacement of the mass, θ is the angle between the membrane in its deflected and undeflected state.

This means that l_0 and z_0 are parameters after the membrane pre-strech in the fabrication process. This influences the hyperelastic model, as will be discussed later. Additionally, as in [13], in the model definition the auxiliary function $\lambda_r^2 = s(d) = 1 + \frac{d^2}{l_0^2}$ is used to simplify the notation.

The vertical force equilibrium on the biasing mass can be defined as:

$$\ddot{d} = g - \frac{2\pi r z}{m} sin(\theta) \left(\sigma_{Maxwell} + \sigma_{Mechanical} \right) \tag{5}$$

where m is the mass of the biasing load, r is the radius of the cylindrical biasing mass m, g means standard gravity, $\sigma_{Maxwell}$, $\sigma_{Mechanical}$ are the Maxwell and mechanical stress.

The electromechanical coupling is produced by Maxwell Stress $\sigma_{Maxwell}$ which compresses the membrane when a voltage is applied to the DEA. The actuation is in the thickness direction and due to the constant volume condition, produces an actuation stretch in the radial direction, λ_r. The value of the Maxwell stress is equal to:

$$\begin{aligned} \sigma_{Maxwell} &= c_2 s(d) u^2 \\ c_2 &= -\frac{\varepsilon_0 \varepsilon_r}{z_0^2} \end{aligned} \tag{6}$$

where ε_0 is vacuum permittivity, ε_r is the relative permittivity of the polymer material and u is the applied voltage. In our approach we consider the actuator as being a perfect capacitor (i.e. we neglect the series resistance of the electrodes). This is possible, as even with an electrode resistance of the order of tens of $\mathrm{k}\Omega$ the electrical cut-off frequency of our actuators (their capacitances is about $1\,\mathrm{nF}$) is orders of magnitude higher than their mechanical bandwidth [13], [33].

The mechanical stress $\sigma_{Mechanical}$ is composed of the viscoelastic stress, empirical viscous damper and hyperelasticity:

$$\sigma_{Mechanical} = \sigma_h + \sigma_{v_1} + \sigma_{v_2} \tag{7}$$

where σ_h is the hyperelastic stress, σ_{v_1} is the viscoelastic stress and σ_{v_2} is the viscous damper stress. The components of mechanical stress are presented in Fig. 2 and are explained in details below. The three parts have different influence on the mechanical behavior, despite the fact that σ_{v_1} and σ_{v_2} represent a generalized Maxwell model.

The DEA membrane has hyperelastic properties as reported in [35], [36]. Many hyperelastic strain energy density functions exist, such as Yeoh, Ogden, Arruda-Boyce, etc. In this work, we use the Ogden model [37]. Similar to [13], we define two parameters β_i and γ_i to integrate the prestretch into the strain energy function:

$$\beta_i = \mu_i \lambda_p^{2i} \tag{8}$$

$$\gamma_i = \mu_i \lambda_p^{-4i}, \tag{9}$$

where $i = 1, 2, 3$ is the index and μ_i is the Ogden model coefficients.

In addition, to reduce the complexity of the model, and based on the experimental data from [13], we have limited the number of elements of the Ogden model to 3.

This leads to the following expression for the hyperelastic stress:

$$\sigma_h = \sum_{i=1}^{3} \left(\beta_i \lambda_r^{2i} - \gamma_i \lambda_r^{-2i} \right). \tag{10}$$

The hyperelastic stress σ_h is presented in Fig. 2 as a part of the mechanical stress.

Viscoelasticity in elastomers is usually modelled with several branches with different time constants corresponding to the different relaxation processes [12], [22], [35]. To identify the number of branches required to accurately model our actuators, we first considered a system with a single relaxation process. However, fittings on experimental data showed that this was not sufficient. We found that an additional branch containing a single dash pot leads to excellent fitting to the experimental data. Additionally, it allows to adequately model the damping of the oscillations. Usually, 3 or more viscoelastic branches are required to accurately model the viscoelastic relaxation of a DEA [12], [22], [35]. We attribute the adequacy of two branches for our actuators to the fact that we are using silicone membranes instead of VHB, which has much less viscous losses. However, the model could easily be expanded to include additional branches, should it be used to model VHB-based actuators. The first part of the viscoelasticity is modeled by a series connection of a viscous damper and an elastic spring as presented in Fig. 2. Hence, the viscoelastic stress is given by:

$$\begin{aligned} \sigma_{v_1} &= -k_1 \epsilon_1 + k_1 (\lambda_r - 1) \\ \dot{\epsilon_1} &= -\frac{k_1}{\eta_1} \epsilon_1 + \frac{k_1}{\eta_1} (\lambda_r - 1) \end{aligned} \tag{11}$$

where ϵ_1 is the strain of the damper in the viscoelasticity model, k_1 is the elastic modulus and η_1 is the viscosity of the material. The term $\lambda_r - 1$ describes the engineering strain of the DEA membrane in the radial direction.

The second part of the viscoelasticity model, which is also shown in Fig. 2, is called the viscous damper and it is given by:

$$\begin{aligned} \sigma_{v_2} &= \eta_2 \dot{\lambda_r} = \eta_2 \varphi(d) \dot{d} \\ \varphi(d) &= \frac{d}{l_0 \sqrt{l_0^2 + d^2}} \end{aligned} \tag{12}$$

where η_2 is the damping coefficient.

This additional stress stems from experimental observation, and leads to a much better fit to experimental data, as exposed in more details in Section IV. Initially, our model contained two viscoelastic branches (spring k_2 in series with a dashpot η_2), as viscoelastic processes with 2 time constants have been reported in the literature [12]. This is especially true if polyurethane or acrylic elastomers (VHB4910) are used as dielectric membranes [38]. However, during our experimental optimization procedures, the time constant η_2/k_2 systematically approached 0, which indicates that the spring constant k_2 converges to infinity. Consequently, we converted the second branch of the viscoelastic model to a purely viscous damper η_2, as shown in Fig. 2. It gives us the possibility to model the resonance frequency and the damping of the oscillations more accurately.

III. HARMONIC BALANCE METHOD

Before attempting to deal with the parameter identification of the DEAs, it is worth discussing the available methods of finding the steady state solution of a DEA model. This is not a trivial task, as DEAs exhibit both slow and fast dynamics. Hence, the response to a sinus excitation can take a long time to converge to steady state. This has motivated researchers to find more efficient tools to search for the steady state solution. An interesting methodology called the Harmonic Balance Method is well known in literature [24]–[27], [29], [39] and can be applied to solve this problem.

In this section, we briefly describe the HBM methodology, based on the literature [25], [26], [29], [39]. The main assumption is that the response of a nonlinear system to an harmonic excitation can be represented by a Fourier Series. Hence the steady state solution $x_s(t)$ can be written as:

$$x_s(t) \approx \sum_{n=-N}^{N} X_n e^{jn\omega t} \tag{13}$$

where j is the imaginary unit, ω is the fundamental frequency of the signal in radians, X_n are the coefficients of the Fourier Series and N is the number of coefficients. If N approaches infinity, the Fourier Series becomes an exact representation of the steady state. Furthermore, it is possible to approximate the derivative of $x_s(t)$ as:

$$\dot{x}_s(t) \approx jn\omega \sum_{n=-N}^{N} X_n e^{jn\omega t} \tag{14}$$

The steady state solution $x_s(t)$ must satisfy the general nonlinear equation $\dot{x} = f(x,u)$ where the function $f(x,u)$ represents the state equation of the model. Hence, the following equation is satisfied:

$$0 \approx jn\omega \sum_{n=-N}^{N} X_n e^{jn\omega t} - f(\sum_{n=-N}^{N} X_n e^{jn\omega t}, u(t)) \tag{15}$$

where $u(t)$ is the harmonic excitation (input signal). If we would like to calculate the response on some harmonic excitation for a system described by $\dot{x} = f(x,u)$, then the steady state solution is the unknown $x_s(t)$. Hence, the coefficients X_n must be found based on (15). The solution of (15) represents a root finding problem, with the main question being how to efficiently calculate the coefficients X_n. In the literature, optimization solvers are applied to find these coefficients, such as the Newton-Krylov nonlinear algebraic solver [29]. Furthermore, there are two approaches in solving a root problem. In the first one, the Fourier transform of the steady state solution is numerically calculated using the fast Fourier transform (FFT) algorithm. Then, the root solving problem searches the solution using the coefficients X_n as in (15). For the second one, the steady state solution is expressed as $x_s(t)$ for fixed set of t values. Then, the FFT is only applied to calculate the approximation of the derivative [40]. Let us denote the approximation of $\dot{x}_s(t)$ found by FFT as $x_s^d(t)$. Then, the root finding problem must be solved for equation:

$$0 \approx x_s^d(t) - f(x_s(t), u(t)) \tag{16}$$

However, in this approach the approximation $x_s^d(t)$ must be calculated in every iteration of the root finding problem solver. In our work, we use the second approach because the optimization algorithm has a faster convergence than in the first approach.

To solve the steady state equation with the HBM, the DEA model is rewritten into a state space form:

$$\dot{x} = f(x,u) \tag{17}$$

where

$$f(x,u) = \begin{bmatrix} \dot{d} \\ -\frac{k_1}{\eta_1}\epsilon_1 + \frac{k_1}{\eta_1}(\lambda_r - 1) \\ g - \bar{c}_1 \frac{d}{s(d)} (\sigma_{Maxwell} + \sigma_{Mechanical}) \end{bmatrix} \tag{18}$$

where $x = \begin{bmatrix} d & \epsilon_1 & \dot{d} \end{bmatrix}^T$ is the state vector and u is the input (the applied voltage). The state space form (17) for the DEA model is found by converting (5). The expression $2\pi r z sin(\theta)$ can be expressed as $\bar{c}_1 \frac{d}{s(d)}$ where $\bar{c}_1 = \frac{2\pi r z_0}{l_0}$. This is a third order system, with the displacement, strain, and velocity as state variables. In our work, we use the HBM to find the solution to a sinusoidal excitation $u(t) = U_m sin(\omega t)$. However, in general the method is also applicable to other forms of harmonic excitations. To find the HBM solution we use the method `hb_time` from the open source `mousai` library [29]. The method searches a steady-state solution $x_s(t)$ for (16), taking into account the harmonic excitation $u(t)$. The method works on time domain points $x_s(t)$ with a fixed set of t values. The number of t values required by `hb_time` depends on the number of harmonics and is equal to $2N+1$.

IV. EXPERIMENTAL VALIDATION

A. DEA fabrication

The model was tested on 3 different actuators (LP1, A1, and A2) to verify its applicability to membranes with different parameters. The actuator LP1 was purchased from Leap Technology and used as received. The actuator was mounted on a 3D printed frame, and its dimensions given in Table I. We fabricated actuators A1 and A2 as follows (Fig. 3): A commercial silicone film (Wacker Elastosil 2030/250) with

a nominal thickness of $50\,\mu\text{m}$ is equibiaxially prestretched (Fig. 3a) and fixed on a circular plastic frame with an internal diameter of $44\,\text{mm}$. The prestretching step is conducted on a radial stretcher as described in [41]. A pressure-sensitive silicone adhesive (ARclad 7876) is used to hold the prestretched membrane on the frames (Fig. 3b). After prestretch, the thickness of the membranes is measured with an interferometer ($27\,\mu\text{m}$ for A1, and $35\,\mu\text{m}$ for A2). It is not possible to precisely control the prestretch with the radial stretcher, but the effective prestretch λ_p of each membrane is calculated using the membrane thickness measured before and after prestretch ($\lambda_p = 1.36$ for A1, and $\lambda_p = 1.19$ for A2). Although prestretching the membrane is not strictly necessary for an actuator that will provide out-of-plane displacement using a biasing system (in this case, a mass), a slight prestretch makes the fabrication process (especially the airbrushing of the electrodes) easier by pre-tensioning the membrane. Two different values of prestretch are used, to test the proposed control method on membranes biased at different points of their stress-stretch behaviour. The compliant electrodes consist of 10% carbon black (Akzo Nobel Ketjenblack EC-600JD) by weight dispersed in a soft silicone (Bluestar Silbione LSR 4305) and dissolved into isooctane to reduce the viscosity of the mixture in order to make it suitable for spray coating. A $50\,\mu\text{m}$-thick Polyethylene naphthalate (PEN) film is cut with a laser plotter to serve as a shadow mask for the spray coating process, defining an annular electrode with an inner diameter of $10\,\text{mm}$ (Fig. 3c). The centre of the actuator, where the biasing mass will later be applied, remains uncoated. An airbrush is used to apply the electrode solution on both sides of the elastomer membrane. Once the PEN masks are removed, the actuator is placed in an oven at $80\,^\circ\text{C}$ for 30 minutes to crosslink the electrodes. Finally, a piece of copper tape is added on each side of the actuator to provide electrical contacts to the electrodes. The DEA is loaded with a mass, which consists of a 3D-printed $4.5\,\text{mm}$ base with a hole for a screw (Fig. 3d). Different screws can be mounted on the base to change the value of the mass.

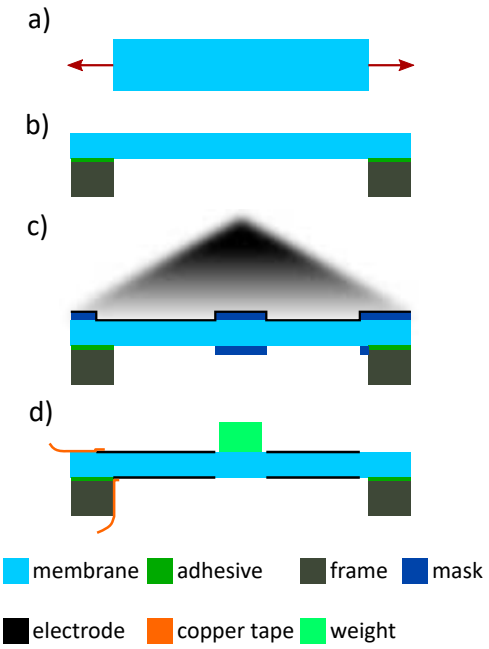

Fig. 3. Fabrication process of the dielectric elastomer actuators. The fabricated devices have a membrane diameter of $44\,\text{mm}$, with a central hub of $9\,\text{mm}$ in diameter. The membrane thickness is about $30\,\mu\text{m}$, with the exact values given in Table I. a) Equi-biaxial prestretch. b) Bonding of membrane on a circular frame using silicone adhesive. c) Spray-coating of the annular electrode through a shadow mask (both sides). d) Addition of the electrical contacts and of the inertial weight.

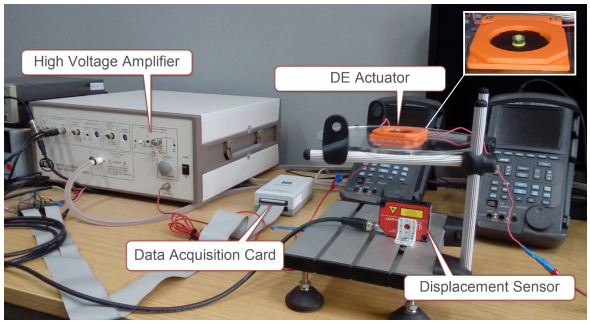

Fig. 4. Measurement set-up for the characterization of the actuators, with a high voltage amplifier, DE actuator, data acquisition card and displacement sensor.

B. Static parameters identification

In this section we present the identification procedure of our DEA model. It is based on an optimization problem. Firstly, a series of experiments were conducted to obtain the responses of our 3 DEA prototypes. The dimensions of the actuators are shown in Table I. The samples were characterised on the experimental set-up shown in Fig. 4. The laboratory set-up consists of a high voltage amplifier TREK MODEL 10/10B-HS, a laser distance sensor Micro-Epsilon optoNCDT ILD1320-10 with $1\,\mu\text{m}$ accuracy, and an Inteco RT-DAC/USB data acquisition card. The results of the step responses for the three membranes are presented in Fig. 5.

The model defined in (5) has mechanical and electromechanical parameters. Due to the nonlinearity of the model, optimization methods were applied to find the model parameters. In the first step, the static measurements were used to find the values of the Ogden model coefficients and relative permittivity. Hence, the following optimization problem is solved:

$$\min_{\beta_1,\beta_2,\beta_3,\gamma_1,\gamma_2,\gamma_3,\epsilon_r} w_m J_m + w_u J_u \tag{19}$$

where w_m and w_u are weight coefficients between two objective functions J_m and J_u. Both functions take into account the steady state of the actuator model. The first function describes the static displacement of the membrane caused by a mass m_k in the absence of voltage. The second function describes the steady state value of the distance d_j caused by the applied voltage u_j, with a constant mass m_u. The objective functions

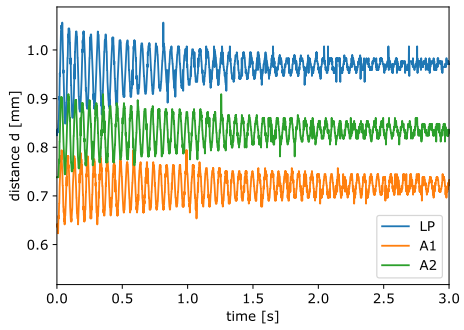

Fig. 5. Displacement versus time for the 3 membranes caused by a voltage step of 2.2 kV.

are defined as:

$$J_m = \sum_{k=1}^{N_k} \left[m_k g - \frac{\overline{c}_1 d_k}{s(d_k)} \underline{\sigma}_e(\lambda_r(d_k)) \right]^2$$
$$J_u = \sum_{j=1}^{N_j} \left[m_u g - \overline{c}_1 c_2 d_j u_j^2 - \frac{\overline{c}_1 d_j}{s(d_j)} \underline{\sigma}_e(\lambda_r(d_j)) \right]^2 . \quad (20)$$

First, we measure the static response without voltage for a mass of 0 and 3 g. Hence, in the goal function we have $N_k = 2$. In a second step, we take into account the steady state response for the following voltages 2.0 kV, 2.1 kV, 2.2 kV, 2.3 kV, 2.4 kV and 2.5 kV ($N_j = 5$) with single mass load $m_u = 3$ g. The choice of our maximal voltage is close to the limit of dielectric breakdown (80 V µm^{-1}–100 V µm^{-1}) of the silicone. However, in the case of different membranes the range of applied voltages can vary. Initially, the weights w_u and w_m were chosen to $\frac{1}{N_j}$ and $\frac{1}{N_k}$ which equalize the effect of both performance indexes. Then, to minimize the optimization error, the weights were adjusted by a trial and error method. The final values were chosen to $w_u = \frac{1}{N_j}$ and $w_m = \frac{0.1}{N_k}$. The optimization problem was run with a Nelder-Mead simplex algorithm [42] using SciPy python package [43]. The results of the optimization is shown in Fig. 6, and it can be seen that the optimization succeeds for each membrane with a very low absolute error (below 3.3 µm, 14.2 µm, 5.5 µm for membrane LP1, A1 and A2 respectively). The hyperelastic parameters based on the Ogden model are visible in Table II. It is worth pointing that the Ogden model parameters β_i and γ_i for A1 and A2 are different, as they include the initial prestrech, see (8) and (9). The relative permittivity of A1 and A2 should be identical, as they are made from the same silicone membrane (Wacker Elastosil Film 2030/250), with a relative permittivity of $\varepsilon_r = 2.8$ according to the product datasheet. The observed difference is most likely caused by phenomena that are not included in our model, such as the impact of the electrodes. However, it does not affect the validity of the results, as our objective is not to use the measurement to extract a precise value of the relative permittivity, but to use the model to predict the dynamic behavior of DEAs.

TABLE I
DIMENSIONS AND PRESTRETCH OF THE 3 ACTUATORS USED FOR THE EXPERIMENTAL VERIFICATION.

Parameter	Symbol	Value			Units
Membrane name		LP1	A1	A2	
Prestretch factor	λ_p	1.15	1.36	1.19	-
Membrane thickness	z_0	38	27	35	µm
Internal plate radius	r	4.5	4.5	4.5	mm
Electrode width	l_0	14	17	17	mm

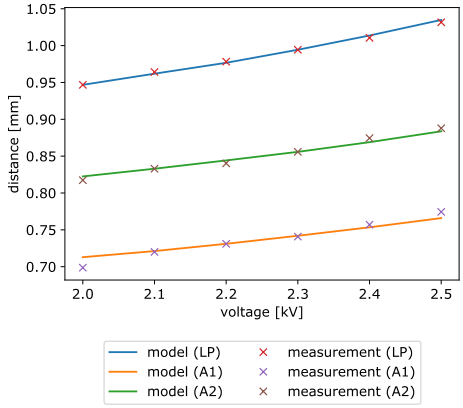

Fig. 6. Steady state vertical displacement of the 3 actuators as a function of applied voltage. Crosses: experimental values, lines: result of the optimization process.

C. Dynamic parameters identification

The main problem encountered with the identification of the dynamics parameters is to obtain the coefficients k_1, η_1 and η_2. These viscoelastic parameters define the transient behavior of the DEA model. Hence additional set of experiments were conducted with sinusoidal voltage excitation. The frequency range was chosen relative to the mechanical bandwidth of the system. Silicone-based DEAs can actuate in the kHz range when the mass of the system is limited to that of the membrane. Due to the addition of the proofmass, the bandwith of our actuator was limited to about 40 Hz. However, we expect the model to work on systems with a lower inertia that can be driven at higher frequencies. The root mean square (RMS) of displacement is calculated from the frequency response measurement by:

$$d_{rms} = \sqrt{\frac{1}{N_T} \sum_{k=1}^{N_T} [d_k - d_0]^2} \quad (21)$$

where N_T is the number of measured points per period, d_0 is the static equilibrium displacement, and d_k is the measured displacement. Thanks to taking d_0 into account, it is possible to compare the response of actuators with different static force-distance characteristics. The results for all membranes are shown in Fig. 7. The measured resonance frequency for the three DEAs were as follows: $f = 8.9$ Hz, $f = 9.6$ Hz, $f = 9.1$ Hz for LP1, A1 and A2. The resonance frequencies

TABLE II
DEA MODEL PARAMETERS

Parameter	Symbol	Value			Units
Membrane name		LP1	A1	A2	
Standard gravity	g	9.81			$\mathrm{m\,s^{-2}}$
Vacuum permittivity	ε_0	$8.85 \cdot 10^{-12}$			$\mathrm{N\,m^{-1}}$
Relative permittivity	ε_r	2.45	2.31	2.63	-
Coefficient of viscoelastic model	k_1	18.41	69.89	40.25	MPa
Coefficient of viscoelastic model	η_1	434.38	5.39	37.58	MPa s
Damping coefficients	η_2	19.42	16.35	35.11	kPa s
Hyperelastic model coefficient	β_1	110	343	-222	kPa
Hyperelastic model coefficient	β_2	-86.7	267	-233	kPa
Hyperelastic model coefficient	β_3	267	-81.8	901	kPa
Hyperelastic model coefficient	γ_1	-43.5	134	524	kPa
Hyperelastic model coefficient	γ_2	-80.3	-396	-504	kPa
Hyperelastic model coefficient	γ_3	-51.3	-245	-265	kPa

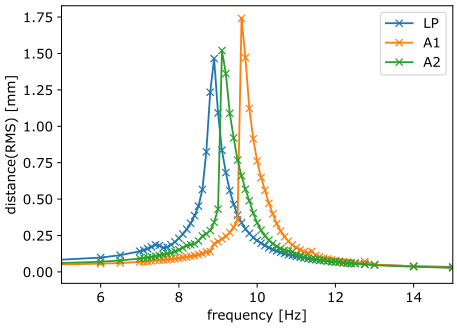

Fig. 7. The comparison of frequency response on sinusoidal input for voltage amplitude $2.5kV$ and various membrane types.

were measured with a sinusoidal input signal of constant amplitude (2.5 kV) and varying frequency.

The optimization procedure for the dynamic parameters is based on both a step response and a frequency response. Hence, the following optimization problem is solved:

$$\min_{k_1,\eta_1,\eta_2} w_{step} \sum_{k=1}^{N_{step}} J_{u_k,step} + w_{hbm} \sum_{k=1}^{N_{hbm}} J_{\omega_k,hbm} \qquad (22)$$

where w_{step} and w_{hbm} are weight coefficients, N_{step} is the number of step responses, N_{hbm} is the number of frequency responses. The performance index $J_{u_k,step}$ is calculated as:

$$J_{u_k,step} = \sum_{j=0}^{N_f} e_d^2(j) \qquad (23)$$

where N_f is a number of samples in experiment, e_d is distance error between simulation and experiment and u_k is the amplitude of the step voltage excitation. The sampling rate of the experiments was 1 ms. The performance index $J_{\omega_k,hbm}$ is calculated from the steady state response to a sinusoidal excitation:

$$J_{\omega_k,hbm} = (d_{m,rms} - d_{s,rms})^2 \qquad (24)$$

where $d_{m,rms}$ is the measured distance (RMS), and $d_{m,rms}$ is the simulated distance (RMS), calculated using (21).

The step response and frequency response are measured on the three DEAs membranes. The transient step response is measured for a voltage of 2.2 kV ($N_{step} = 1$). The frequency response is measured for a wide range of frequencies (from 0.2 Hz to 40 Hz, at a constant voltage amplitude of 2.5 kV). For each step of the optimization, the responses were calculated by numerical forward-integration based on the Runge-Kutta method for the step response, and by the Harmonic Balance Method for the frequency response. Due to performance considerations, only a small subset of frequencies is taken into account for the optimisation f_k =0.2 Hz, 8.3 Hz, 11.2 Hz and 40 Hz. The set of frequency consists of points for frequencies below, around and above resonance as visible in Fig. 7. Hence, we define crucial points of frequency characteristic which we want to fit in the identification process. The weight coefficient are set to ($w_{step} = 6.6 \times 10^6$ and $w_{hbm} = 0.1 \times 10^6$) to scale the performance indexes around 1. Eq. (22) was solved with the Nelder-Mead algorithm from the Python package SciPy [43], [44]. The absolute error of the optimization variable and absolute error of the function between iterations is set to 5×10^{-2} to improve the accuracy. Regarding the optimization variables: coefficients of the viscoelastic model k_1 and η_1, the damping coefficient η_2 are normalized with the following weights: 10^7, 10^8 and 10^4 respectively. We have chosen the initial values of the simplex by a trial and error method. The parameters found in the optimization are shown in Table II.

The characteristics of the responses are presented in Fig. 8. It can be seen that for all three membranes, the step response and frequency response predicted by our model is in excellent agreement with the experimental data. In Table

III we present the performance indexes of the identification error for various membranes calculated from the step responses presented in Fig. 8. We calculated the Integral Absolute Error (IAE), Integral Square Error (ISE), Integral Time Absolute Error (ITAE) to show the quality of identification for different membranes. In Table IV the peak of the resonance frequency is compared for the simulations and measurements. We have verified the ability of the model to accurately capture the viscoleastic behaviour of the actuators by submitting our test devices to a sinusoidal voltage input with a frequency of $2\,\mathrm{Hz}$ and $12.5\,\mathrm{Hz}$. Our viscoelastic model is in excellent agreement with the experimental data.

TABLE III
PERFORMANCE INDEXES INTEGRAL ABSOLUTE ERROR (IAE), INTEGRAL SQUARE ERROR (ISE), INTEGRAL TIME ABSOLUTE ERROR (ITAE) FOR IDENTIFICATION ERROR BETWEEN MODEL AND EXPERIMENT FOR STEP RESPONSE.

Performance Index	Value		
Membrane name	LP1	A1	A2
IAE $[\mathrm{mm\,s}]$	0.137	0.0923	0.084
ISE $[\mathrm{mm^2\,s}]$	0.0033	0.00195	0.0018
ITAE $[\mathrm{mm\,s^2}]$	0.5173	0.2793	0.2497

TABLE IV
THE DIFFERENCE BETWEEN THE RESONANCE PEAK IN THE SIMULATIONS AND MEASUREMENTS FOR THE VARIOUS MEMBRANES.

	Resonance peak [Hz]		Error
Method	Simulation	Measurement	
LP1	9.3	8.9	4.5 %
A1	10.2	9.6	6.25 %
A2	9.5	9.1	4.4 %

D. Analysis of η_2

The viscoelasticity is important phenomenon for DEA membranes. In our model we describe viscoelasticity with the coefficients k_1, η_1 and η_2. The influence of different values of η_2 (12) on the model is shown in Fig. 9. The model is simulated based on the parameters of membrane A1 with three different values of η_2. The analysis is performed for a step response for a voltage of $2.2\,\mathrm{kV}$ and calculated by forward integration. It is clearly visible that the damping coefficient η_2 controls the damping of the oscillations. The existence of the second time constant is required as it is responsible for large time scale behavior.

E. Performance of the HBM solver

The performance of the solver is a crucial issue in the identification of the parameters by an optimization approach. As long as the optimization algorithm needs to compute the steady state response of the actuator for each iteration, the performance of solver is critical. Hence, the number of iterations required to find the steady state solution by the HBM was studied for different numbers of harmonics. The simulations were run for the DEA with membrane A2 based on the parameters in Table II. The input voltage was sinus with $2.5\,\mathrm{kV}$ amplitude. The frequency range was $0.1\,\mathrm{Hz}$–$20\,\mathrm{Hz}$. In Fig. 10, it is visible that the performance of the HBM varies with the frequency of the excitation voltage. The worst performance is observed close to the resonance frequency. Furthermore, the higher number of harmonics leads to a lower performance. However, this is the cost of a better accuracy. The HBM approach is also compared with the forward integration method (Runge-Kutta [45]). In this case the number of iterations is constant, because we need to integrate until the system has reached steady state. Additionally, the time when transient is finished can be unknown. Hence, this can lead to unnecessary overestimation of the number of required iterations. It is visible that for many of the frequencies, the HBM method provides better performance than solving the ordinary differential equation by integration. In the Table V the median time of execution was calculated for Harmonic Balance Method (HBM) and Forward Integration (FI). It is visible that the median of time execution for the Harmonic Balance Method is significantly lower than for Forward Integration. Additionally, we have analyzed the accuracy of the HBM solver with respect to the FI solution as a function of the number of harmonics, in order to evaluate the balance between accuracy and computational cost. The analysis is made for a set of frequencies ($0\,\mathrm{Hz}$–$20\,\mathrm{Hz}$) and the HBM was computed for 2,4,6,8 harmonics. The RMS of displacement (21) was calculated for each response. We have defined the error as:

$$e_{accuracy} = \frac{|d_{rms,HBM} - d_{rms,FI}|}{d_{rms,FI}} \times 100\% \qquad (25)$$

where $d_{rms,HBM}$, $d_{rms,FI}$ is the RMS of displacement for the HBM and FI methods respectively. The accuracy results can be grouped into two regions: around the resonance frequency and away from the resonance frequency. In the first case the number of harmonics has influences the error. The mean error for a set of frequencies $0.5\,\mathrm{Hz}$ around resonance is presented in column accuracy in Table V. In the second case the error is almost everywhere below 1%, irrespective of the number of harmonics. From this, we can conclude that for this particular case, using 6 harmonics is a good tradeoff between computation time and accuracy, as using 8 harmonics comes at the cost of a much longer computing time for no improvements in accuracy. If an application is known to use input frequencies which stay away from the resonance region, then 2 harmonics will be enough and combine the advantage of a high accuracy with a low computing time.

V. CONCLUSIONS

A complex dynamic model is necessary to account for the capacitive and viscoelastic properties of DEAs. In this paper a nonlinear model was derived by combining an electrical circuit model with an Ogden hyperelastic model taking into account viscous damping forces. Since DEAs can be regarded as

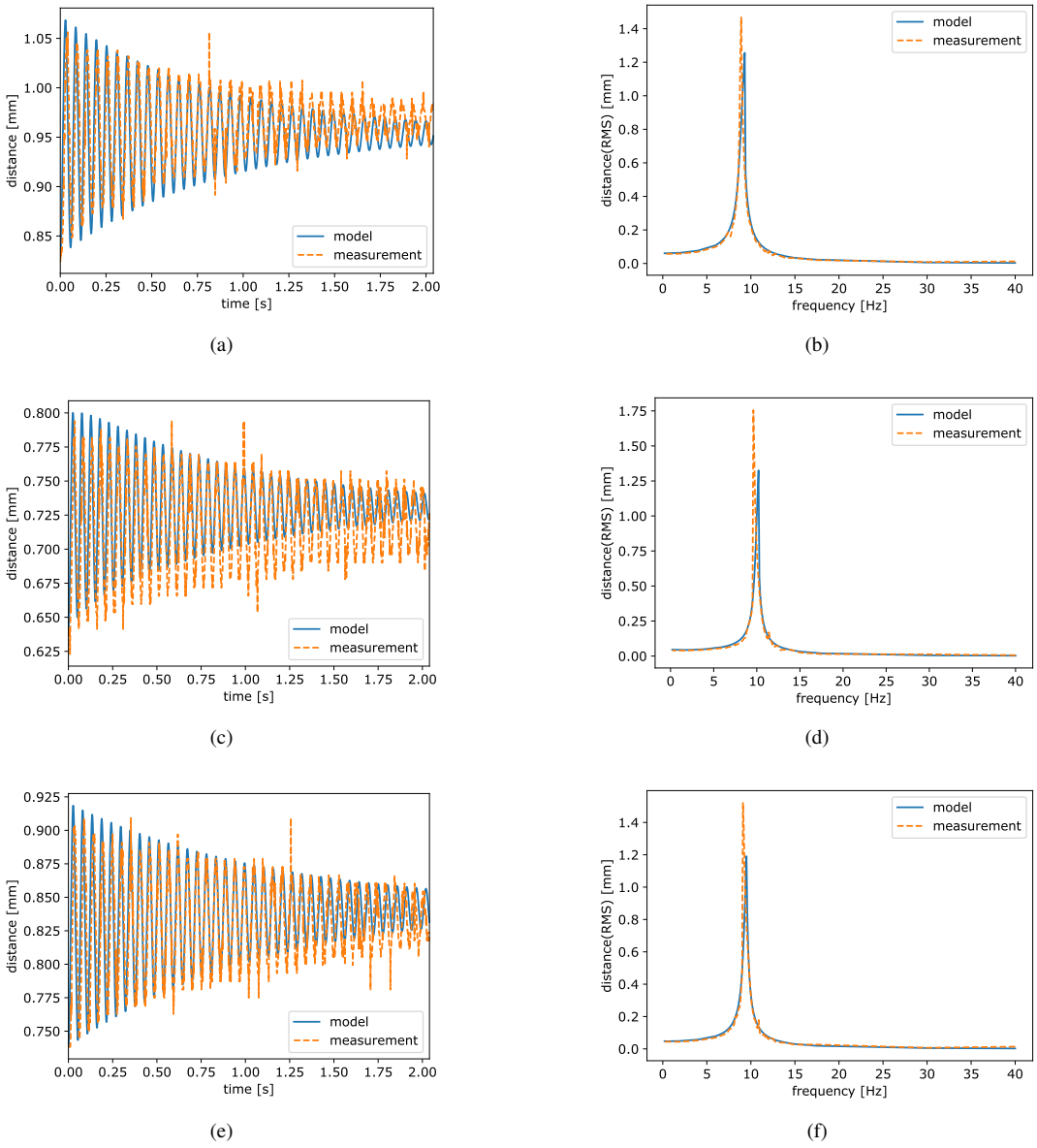

Fig. 8. Comparison of the step responses (left) and frequency characteristics (right) between experiments and simulations. LP1 (a,b), A1 (c,d), A2 (e,f).

deformable capacitors, applying a time-varying stimulus introduces a time-dependent and frequency-dependent mechanical response. Our model, which relies on an identification process to quickly find the model parameters, can adequately capture both phenomena. We have shown that the model is in close agreement with the measured responses of the real DEA, and that the use of the HBM method enables us to identify the model parameters 2 order of magnitude faster than a forward-integration method.

APPENDIX A
ACKNOWLEDGMENT

This work was realized with the frame of project SONATA 13 No. 2017/26/D/ST7/00092 from National Science Centre (Poland). The authors wish to thank Wacker Chemie AG and Dr. Andreas Koellnberger for providing the Elastosil membranes used to make actuators A1 and A2.

REFERENCES

[1] K. Kim and T. S., *Electroactive Polymers for Robotics Applications: Artifical Muscles and Sensors*. Springer, 2007.

[2] Y. Bar-Cohen, *Electroactive polymer (EAP) actuators as artificial muscles: reality, potential, and challenges*. Bellingham: SPIE Press, 2001.

[3] Z. Suo, "Theory of dielectric elastomers," *Acta Mechanica Solida Sinica*, vol. 23, no. 6, pp. 549–578, 2010.

[4] X. Zhao and Q. Wang, "Harnessing large deformation and instabilities of soft dielectrics: Theory, experiment, and application," *Applied Physics Reviews*, vol. 1, no. 2, 2014.

[5] F. Carpi, I. Anderson, S. Bauer, G. Frediani, G. Gallone, M. Gei, C. Graaf, C. Jean-Mistral, W. Kaal, G. Kofod, M. Kollosche, R. Kornbluh, B. Lassen, M. Matysek, S. Michel, S. Nowak, B. O'Brien, Q. Pei, R. Pelrine, B. Rechenbach, S. Rosset, and H. Shea, "Standards for dielectric elastomer transducers," *Smart Materials and Structures*, vol. 24, no. 10, 2015.

[6] R. Pelrine, R. Kornbluh, Q. Pei, and J. Joseph, "High-speed electrically actuated elastomers with strain greater than 100%," *Science*, vol. 287, no. 5454, pp. 836–839, 2000.

[7] J.-S. Plante and S. Dubowsky, "Large-scale failure modes of dielectric

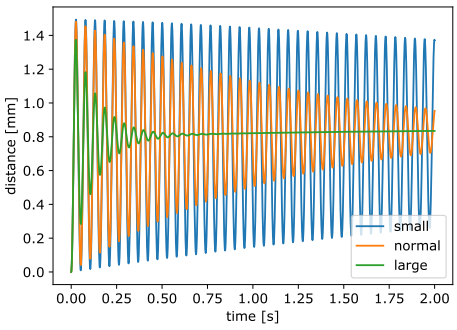

Fig. 9. The analysis of influence of coefficient η_2 on the DEA model for 2.2 kV step voltage. The small, normal and large value of damping coefficient are $0.1\eta_2$, $1\eta_2$ and $10\eta_2$ respectively.

TABLE V
THE MEDIAN OF TIME EXECUTION AND ACCURACY FOR HARMONIC BALANCE METHOD (HBM) AND FORWARD INTEGRATION (FI). THE LAST COLUMN SHOWS THE RELATIVE ERROR AROUND RESONANCE OF THE HBM WITH RESPECT TO FI. OUTSIDE OF THE RESONANCE ZONE, THE ERROR IS LOWER THAN 1%.

Number of harmonics	Median execution time [s]		Gain	Accuracy
	HBM	FI		
2	0.0653	23.027	352.6	5.3 %
4	0.0897	23.090	257.8	4.2 %
6	0.1520	22.350	147.0	3.4 %
8	0.4857	22.516	46.4	3.4 %

elastomer actuators," *International Journal of Solids and Structures*, vol. 43, no. 25-26, pp. 7727–7751, 2006.

[8] I. Anderson, T. Gisby, T. McKay, B. O'Brien, and E. Calius, "Multi-functional dielectric elastomer artificial muscles for soft and smart machines," *Journal of Applied Physics*, vol. 112, no. 4, 2012.

[9] M. Hodgins, G. Rizzello, A. York, and S. Seelecke, "High-frequency dynamic model of a pre-loaded circular dielectric electro-active polymer actuator," vol. 2, 2013.

[10] S. Rosset and H. Shea, "Small, fast, and tough: Shrinking down integrated elastomer transducers," *Applied Physics Reviews*, vol. 3, no. 3, 2016.

[11] W. Kaal and S. Herold, "Electroactive polymer actuators in dynamic applications," *IEEE/ASME Transactions on Mechatronics*, vol. 16, no. 1, pp. 24–32, 2011.

[12] R. Sarban, B. Lassen, and M. Willatzen, "Dynamic electromechanical modeling of dielectric elastomer actuators with metallic electrodes," *IEEE/ASME Transactions on Mechatronics*, vol. 17, no. 5, pp. 960–967, 2012.

[13] G. Rizzello, D. Naso, A. York, and S. Seelecke, "Modeling, identification, and control of a dielectric electro-active polymer positioning system," *IEEE Transactions on Control Systems Technology*, vol. 23, no. 2, pp. 632–643, 2015.

[14] G. Berselli, R. Vertechy, M. Babič, and V. P. Castelli, "Dynamic modeling and experimental evaluation of a constant-force dielectric elastomer actuator," *Journal of Intelligent Material Systems and Structures*, vol. 24, no. 6, pp. 779–791, 2013.

[15] A. Rajamani, M. Grissom, C. Rahn, and Q. Zhang, "Wound roll dielectric elastomer actuators: Fabrication, analysis, and experiments," *IEEE/ASME Transactions on Mechatronics*, vol. 13, no. 1, pp. 117–124, 2008.

[16] F. Carpi, C. Menon, and D. De Rossi, "Electroactive elastomeric actuator for all-polymer linear peristaltic pumps," *IEEE/ASME Transactions on Mechatronics*, vol. 15, no. 3, pp. 460–470, 2010.

[17] R. Vertechy, G. Berselli, and V. Castelli, "Electro-elastic model for dielectric elastomers," *Mechanisms and Machine Science*, vol. 14, pp. 245–250, 2013.

[18] G. Berselli, G. Mammano, and E. Dragoni, "Design of a dielectric elastomer cylindrical actuator with quasi-constant available thrust: Modeling procedure and experimental validation," *Journal of Mechanical Design, Transactions of the ASME*, vol. 136, no. 12, 2014.

[19] M. Babič, R. Vertechy, G. Berselli, J. Lenarčič, V. Parenti Castelli, and G. Vassura, "An electronic driver for improving the open and closed loop electro-mechanical response of dielectric elastomer actuators," *Mechatronics*, vol. 20, no. 2, pp. 201–212, 2010.

[20] S. Schlatter, P. Illenberger, and S. Rosset, "Peta-pico-voltron: An open-source high voltage power supply," *HardwareX*, vol. 4, 2018.

[21] T. Soderstrom and P. Stoica, *System Identification*. Prentice Hall, 1989.

[22] J. Zou and G. Gu, "Dynamic modeling of dielectric elastomer actuators with a minimum energy structure," *Smart Materials and Structures*, vol. 28, no. 8, 2019.

[23] U. Gupta, Y. Wang, H. Ren, and J. Zhu, "Dynamic modeling and feedforward control of jaw movements driven by viscoelastic artificial muscles," *IEEE/ASME Transactions on Mechatronics*, vol. 24, no. 1, pp. 25–35, 2019.

[24] R. Genesio and A. Tesi, "Harmonic balance methods for the analysis of chaotic dynamics in nonlinear systems," *Automatica*, vol. 28, no. 3, pp. 531–548, 1992.

[25] R. Mickens, *Truly nonlinear oscillations: Harmonic balance, parameter expansions, iteration, and averaging methods*, 2010.

[26] K. Sanliturk and D. Ewins, "Modelling two-dimensional friction contact and its application using harmonic balance method," *Journal of Sound and Vibration*, vol. 193, no. 2, pp. 511–523, 1996.

[27] C. Pierre, A. Ferri, and E. Dowell, "Multi-harmonic analysis of dry friction damped systems using an incremental harmonic balance method." *TRANS. ASME J. APPL. MECH.*, vol. 52, no. 4 , Dec. 1985, pp. 958–964, 1985.

[28] T. Öziş and A. Yildirim, "Determination of the frequency-amplitude relation for a duffing-harmonic oscillator by the energy balance method," *Computers and Mathematics with Applications*, vol. 54, no. 7-8, pp. 1184–1187, 2007.

[29] J. C. Slater, "Mousai: An open source harmonic balance solver for nonlinear systems," in *13th ASME Dayton Engineering Sciences Symposium*, Oct. 30 2017.

[30] Z. Wang and T. He, "Electro-viscoelastic behaviors of circular dielectric elastomer membrane actuator containing concentric rigid inclusion," *Applied Mathematics and Mechanics (English Edition)*, vol. 39, no. 4, pp. 547–560, 2018.

[31] Y. Li, I. Oh, J. Chen, H. Zhang, and Y. Hu, "Nonlinear dynamic analysis and active control of visco-hyperelastic dielectric elastomer membrane," *International Journal of Solids and Structures*, 2018.

[32] G. Rizzello, M. Hodgins, D. Naso, A. York, and S. Seelecke, "Modeling of the effects of the electrical dynamics on the electromechanical response of a DEAP circular actuator with a mass–spring load," *Smart Materials and Structures*, vol. 24, no. 9, p. 094003, aug 2015.

[33] G. Rizzello, D. Naso, B. Turchiano, and S. Seelecke, "Robust position control of dielectric elastomer actuators based on lmi optimization," *IEEE Transactions on Control Systems Technology*, vol. 24, no. 6, pp. 1909–1921, 2016.

[34] J. Bernat and J. Kolota, "Adaptive observer for state and load force estimation for dielectric electro-active polymer actuator," in *11th IFAC Symposium on Nonlinear Control Systems*, September 2019.

[35] M. Wissler and E. Mazza, "Mechanical behavior of an acrylic elastomer used in dielectric elastomer actuators," *Sensors and Actuators, A: Physical*, vol. 134, no. 2, pp. 494–504, 2007.

[36] T. He, L. Cui, C. Chen, and Z. Suo, "Nonlinear deformation analysis of a dielectric elastomer membrane–spring system," *Smart Materials ans Structures*, vol. 19, no. 8, pp. 085 017–1–085 017–7, 2010.

[37] R. W. Ogden, "Large deformation isotropic elasticity – on the correlation of theory and experiment for incompressible rubberlike solids," *Proceedings of the Royal Society of London. Series A, Mathematical and Physical Sciences*, vol. 326, no. 1567, pp. 565–584, 1972.

[38] S. Hau, G. Rizzello, and S. Seelecke, "A novel dielectric elastomer membrane actuator concept for high-force applications," *Extreme Mechanics Letters*, vol. 23, pp. 24–28, 2018.

[39] R. Gilmore and M. Steer, "Nonlinear circuit analysis using the method of harmonic balance—a review of the art. part i. introductory concepts," *International Journal of Microwave and Millimeter-Wave Computer-Aided Engineering*, vol. 1, no. 1, pp. 22–37, 1991.

[40] J. Izaac and J. Wang, *The Fourier Transform*. Cham: Springer International Publishing, 2018, pp. 309–356.

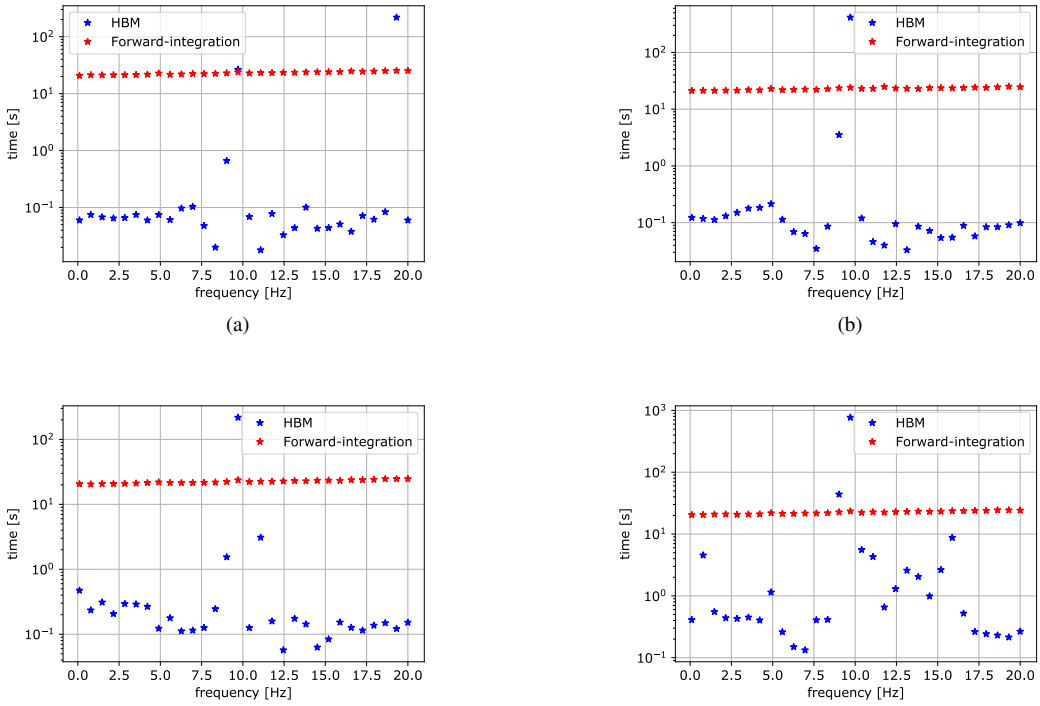

Fig. 10. The time required to find steady state solution by Harmonic Balance Method and Forward Integration. The Harmonic Balance Method was calculated with 2 harmonics (a), 4 harmonics (b), 6 harmonics (c), 8 harmonics (d).

[41] S. Rosset, O. A. Araromi, S. Schlatter, and H. Shea, "Fabrication process of silicone-based dielectric elastomer actuators," *Journal of Visualized Experiments*, vol. 108, no. e53423, pp. 1–13, 2016.
[42] J. A. Nelder and R. Mead, "A simplex method for function minimization," *Comput. J.*, vol. 7, pp. 308–313, 1965.
[43] P. Virtanen, R. Gommers, T. E. Oliphant, M. Haberland, T. Reddy, D. Cournapeau, E. Burovski, P. Peterson, W. Weckesser, J. Bright, S. J. van der Walt, M. Brett, J. Wilson, K. Jarrod Millman, N. Mayorov, A. R. J. Nelson, E. Jones, R. Kern, E. Larson, C. Carey, İ. Polat, Y. Feng, E. W. Moore, J. Vand erPlas, D. Laxalde, J. Perktold, R. Cimrman, I. Henriksen, E. A. Quintero, C. R. Harris, A. M. Archibald, A. H. Ribeiro, F. Pedregosa, P. van Mulbregt, and S. . . Contributors, "SciPy 1.0: Fundamental Algorithms for Scientific Computing in Python," *Nature Methods*, vol. 17, pp. 261–272, 2020.
[44] F. Gao and L. Han, "Implementing the nelder-mead simplex algorithm with adaptive parameters," *Computational Optimization and Applications*, vol. 51, no. 1, pp. 259–277, 2012.
[45] E. Hairer, S. Norsett, and G. Wanner, *Solving Ordinary Differential Equations i. Nonstiff Problems. 2nd edition. Springer Series in Computational Mathematics*. Springer-Verlag, 1993.

Jakub Bernat received the M.Sc. degree in 2007 and the Ph.D. degree in 2011, both from the Poznan University of Technology. He is currently a post-doctoral fellow in the Faculty of Computer Science, Poznan University of Technology. His main research areas are control theory, adaptive systems, robust control and state estimation. Currently he is working on control of electroactive polymers and nonlinear adaptive control.

Jakub Kolota received the M.Sc. degree from Poznan University of Technology, Poland, in 2005, and the Ph.D. degree from the same university in 2009. He is presently a Research Scientist in the Informatics Department, Poznan University of Technology in Poland. His research interests include nonlinear electromagnetic field analysis and synthesis, PLC controllers, cloud computing and control theory in smart materials. In PhD thesis, he described a complex simulation of stepper motor, represented in 3D space with distributed parameters. Currently he is working with electroactive polymers like IPMC and DEAP.

Samuel Rosset received the MSc and PhD degrees in microengineering from the EPFL, Switzerland, in 2004 and 2009, respectively. He is a research fellow at the Auckland Bioengineering Institute at the University of Auckland, New Zealand. He has been working on soft transducers since 2005, with a focus on optical and biomedical applications, as well as on the fabrication processes of these devices. He has authored and co-authored more than 40 peer-reviewed papers.